British Geological Survey

NATURAL ENVIRONMENT RESEARCH COUNCIL

The Dudley Earthquake of 22 September, 2002

Earthquake & Forensic Seismology and Geomagnetism Programme
Internal Report IR/03/113

BRITISH GEOLOGICAL SURVEY

INTERNAL REPORT IR/03/113

The Dudley Earthquake of 22 September, 2002

B. Baptie, L. Ottemoller, S. Sargeant, G. Ford and A O'Mongain

Key words

Hypocentre, focal mechanism, aftershock, peak ground acceleration.

Front cover

Cover picture details, delete if no cover picture.

Bibliographical reference

B. BAPTIE, L. OTTEMOLLER, S. SARGEANT, G. FORD, A. O'MONGAIN. 2003, The Dudley Earthquake of 22 September, 2003. *British Geological Survey Internal Report*, IR/03/113. 1pp.

Keyworth, Nottingham British Geological Survey 2003

BRITISH GEOLOGICAL SURVEY

The full range of Survey publications is available from the BGS Sales Desks at Nottingham and Edinburgh; see contact details below or shop online at www.thebgs.co.uk

The London Information Office maintains a reference collection of BGS publications including maps for consultation.

The Survey publishes an annual catalogue of its maps and other publications; this catalogue is available from any of the BGS Sales Desks.

The British Geological Survey carries out the geological survey of Great Britain and Northern Ireland (the latter as an agency service for the government of Northern Ireland), and of the surrounding continental shelf, as well as its basic research projects. It also undertakes programmes of British technical aid in geology in developing countries as arranged by the Department for International Development and other agencies.

The British Geological Survey is a component body of the Natural Environment Research Council.

Keyworth, Nottingham NG12 5GG

(0115-936 3241 Fax 0115-936 3488
e-mail: sales@bgs.ac.uk
www.bgs.ac.uk
Shop online at: www.thebgs.co.uk

Murchison House, West Mains Road, Edinburgh EH9 3LA

(0131-667 1000 Fax 0131-668 2683
e-mail: scotsales@bgs.ac.uk

London Information Office at the Natural History Museum (Earth Galleries), Exhibition Road, South Kensington, London SW7 2DE

(020-7589 4090 Fax 020-7584 8270
(020-7942 5344/45 email: bgslondon@bgs.ac.uk

Forde House, Park Five Business Centre, Harrier Way, Sowton, Exeter, Devon EX2 7HU

(01392-445271 Fax 01392-445371

Geological Survey of Northern Ireland, 20 College Gardens, Belfast BT9 6BS

(028-9066 6595 Fax 028-9066 2835

Maclean Building, Crowmarsh Gifford, Wallingford, Oxfordshire OX10 8BB

(01491-838800 Fax 01491-692345

Parent Body

Natural Environment Research Council, Polaris House, North Star Avenue, Swindon, Wiltshire SN2 1EU

(01793-411500 Fax 01793-411501
www.nerc.ac.uk

Abstract

The 4.7 ML Dudley earthquake on 22 September 2002 at 23:53 (UTC) was widely felt throughout England and Wales and was the largest earthquake to occur onshore in the United Kingdom (UK) since the magnitude 5.1 ML Bishop's Castle earthquake in 1990. The earthquake hypocentre, determined from inversion of observed P- and S-wave travel-time data suggests a source depth of 14 km and this depth estimate is also supported by forward modelling of observed waveforms. Focal mechanisms obtained from both first motion polarities of local observations and moment tensor inversion of regional observations show left-lateral strike-slip faulting along a near vertical, near north-south striking fault plane whose orientation is in good agreement with the surface expression of the observed faults in the region. Two aftershocks were recorded within the location error ellipsoid of the mainshock. Comparison of the waveform signals revealed that the mainshock and aftershocks were nearly co-located and possibly had the same source mechanism. The observed peak ground acceleration is found to be less than that predicted using five empirical relations, which have been considered applicable in the UK. Seismic moment M_0 and stress drop $\delta\sigma$ were measured from on-scale records where L_g arrivals were clear, and then used to give better estimates of the peak ground accelerations using a stochastic approach.

Introduction

The Dudley earthquake on 22 September 2002 at 23:53 (UTC) was widely felt throughout England and Wales and was the largest earthquake to occur onshore in the United Kingdom (UK) since the magnitude 5.1 ML Bishop's Castle earthquake in 1990 (Ritchie et al., 1990). The epicentre was about 3 km northwest of the town of Dudley in the West Midlands and the Richter local magnitude was determined as 4.7 ML. The UK is a country of low to moderate seismicity and the spatial distribution of earthquakes is generally diffuse, in keeping with other intra-plate areas. Main et al. (1999) suggest a maximum magnitude for UK earthquakes in the range 6.3-7.5 ML based on the observed Gutenberg-

Richter frequency-magnitude law. By comparison, the observed maximum is the magnitude 6.1 ML Dogger Bank earthquake of 1931 (Neilson et al., 1986). The recurrence relationship found by Musson (1994), based on the historical and instrumental earthquake catalogue for the UK, suggests that, on average, earthquakes of magnitude 4.7 ML, or greater, occur somewhere in the UK once in every ten years. Comparable events with respect to magnitude have been the Carlisle earthquake in 1979, the Skipton earthquake in 1944 (Burton et al., 1984), the North Wales earthquake in 1940 (Musson et al., 1984), and the Caernarvon earthquake in 1903 (Musson et al., 1984). Figure 1 shows the instrumental and historical seismicity of the West Midlands from 1700 to the present, in a 100 km square centred on the 2002 epicentre. Prior to 1970, the historical earthquake catalogue is expected to be reasonably complete for earthquakes greater than magnitude 4.0. The seismicity in this region is generally diffuse, although, to the north and east of the 2002 epicentre, the seismicity seems to follow a roughly north-northwest trend through Stafford. The largest earthquake in this area in the last hundred years was the 15 August 1926, 4.8ML, event near Ludlow, causing some minor damage, mostly to chimneys in the epicentral area. More recently, a magnitude 4.2 ML earthquake occurred near Warwick on 23 September 2000.

A map of macroseismic intensity is shown in Figure 2. Intensity values were determined from over 8000 responses to questionnaires published in both a national newspaper and on the Internet. The highest intensity experienced was 5 EMS (European Macroseismic Scale), which was observed in the area around Dudley, Birmingham, Walsall and Wolverhampton, and as far south as Kidderminster and Bromwich. The total felt area, as defined by an intensity of 3 EMS, was 126,000 km^2.

The earthquake was recorded throughout the UK, at seismograph stations operated by BGS (Simpson, 2002), and also regionally on broadband instrumentation operated by other agencies on mainland Europe. Figure 3 shows the locations of seismograph stations used in subsequent analyses and mentioned specifically in the text. Much of the data recorded on the high gain instrumentation operated by BGS was saturated, however, recordings made on lower gain instrumenta-

tion allowed accurate analysis of waveforms at a number of stations. Figure 4 shows the seismograms of the vertical component of ground displacement at five low gain stations in the UK at epicentral distances ranging from 100 to 250 km. Numerous phases are observed throughout the record in addition to direct P-wave and L_g arrivals, possibly associated with Moho and mid-crust refractions and reflections. Regional broadband waveforms were used by researchers at the Swiss Seismological Service to determine a moment tensor solution for the source mechanism using full waveform modelling (Nabelek and Xia, 1995). The event was also observed at teleseismic distances on seismic array stations. Observations from the BGS network on mainland UK and Northern Ireland have been supplemented by data from seismograph stations operated by Keele University, the Atomic Weapons Establishment (AWE) at Blacknest and also IRIS. Two aftershocks were recorded, the first on 23 September at 03:32 (2.7 ML) about 3.5 hours after the main shock and the second on 24 September at 09:29 (1.2 ML), some 30 hours later. Both these events were located within the error ellipsoid of the main shock.

The UK lies on the northwest European shelf and at the northeast margin of the North Atlantic Ocean. Its continental crust formed over a long period of time and has a complex tectonic history, with multiple episodes of deformation resulting in extensive faulting. No British earthquake recorded either historically or instrumentally has produced a surface rupture and typical fault dimensions for UK earthquakes are of the order of 1-2 km. Therefore, it is difficult to accurately map earthquakes to specific faults, particularly at depth, where the fault distributions and orientations are unclear, given the large uncertainties involved. In this work we present location and source parameters determined using common observatory practice for the Dudley main-shock and aftershocks. These results are discussed in the context of the tectonic setting and observed surface faulting. Waveform modelling of high frequency near-source recordings is used to examine the depth constraint of the earthquake hypocentre. In addition we examine the decay of peak ground acceleration with distance and compare this to the peak ground acceleration given by attenuation laws that are considered applicable to the UK. We then use a stochastic method to model peak ground acceleration as a function of distance for the mainshock and largest aftershock, using the

seismic moment and Brune stress drop parameter determined from corrected displacement spectra. A first approximation of PHGA in the near-field is also made.

Geological Setting

A wedge-shaped basement block of Proterozoic crust called the Midlands Microcraton dominates much of Southern Britain (Pharaoh et al., 1993), and is terminated by the Variscan Front to the south and Welsh Caledonides to the North. The geological background of the West Midlands is summarised by Powell et al. (1992). A wide variety of sedimentary rocks were deposited over the time period between 430-225 Ma ago and then subjected to folding, uplift and erosion several times following the Caledonian Orogeny, approximately 380 Ma ago. The final deformation phase (in the Permian) resulted in the Triassic sedimentary strata to the west and east of the Western and Eastern Boundary faults, respectively, being downthrown, defining the West Midlands Coalfield (Figure 5). These faults are two of the numerous normal and reverse faults in the region, many of which dip steeply at the surface. More recently, periods of glaciation and intensive industrial development since the eighteenth century have had a significant effect on the near-surface geology of the West Midlands. Mineral deposits of coal, dolerite and limestone have been exploited extensively. As a result, there are significant areas of made ground. Dudley-Sedgely and Walsall are built above small limestone quarries and larger sub-surface caverns which are either open or partially back-filled.

Earthquake Location

The Dudley earthquake was located using local recordings from the BGS network of seismograph stations. Keele University and AWE Blacknest provided additional data. *P*-wave arrivals were picked on vertical component seismometers and *S*-wave arrivals on three-component seismometers where possible. In-

dividual phases were assigned weightings based on a confidence level in the observed data and the weighted arrival time data were input to the HYPOCENTER location algorithm (Lienert et al., 1988) to determine the earthquake hypocentre. In the absence of any definitive crustal velocity model for this area, from refraction or other sources, we used the 1-D velocity model shown in Table 1, determined from the LISPB refraction experiment (Bamford et al., 1978; Assumpção and Bamford, 1978), over Northern Britain. Strictly speaking, this model is only valid for the Midland valley region of Scotland and contains a near-surface low-velocity zone; however, the model has been widely used to locate earthquakes throughout England and has given reasonable results. An additional weighting factor based on the distance parameters $xnear$ and $xfar$, where the weight is linearly decreased from 1 to 0 between $xnear$ and $xfar$, was used to systematically reduce weighting with distance and is typically applied to reflect lateral heterogeneity in the velocity model. In this case $xnear$ of 100 km and $xfar$ value of 300 km were applied. A total of 54 phase readings were used to determine the earthquake hypocentre, giving an epicentre location of 52.526°N and 2.153°W, about 3 km northwest of Dudley, with horizontal errors of 1.6 km and 2.6 km in the north-south and east-west directions respectively. Figure 6 shows horizontal and vertical projections of the 90% confidence ellipsoid for the calculated hypocentre. The overall RMS error in the hypocentral estimate is 0.33 s and the azimuthal gap is 34°. Figure 7 shows reduced P-wave travel-times for the Dudley earthquake as a function of epicentral distance for both observed (grey circles) and modelled data. The theoretical P-wave travel-times for the primary crustal phases are determined for the 1-D velocity model used to locate the earthquake. The travel-time curves provide a reasonable match to the observed data, with the modelled P_n phase providing a good fit to the data to epicentral distances of about 250 km.

The source depth was determined at 12.9 km with a corresponding error of 3.7 km. However, the nearest seismograph station to the epicentre is 58 km to the north-northeast and the nearest three-component seismograph station that recorded unsaturated P-wave and S-wave arrivals was 80 km to the south-west. In addition, considering the uncertainties associated with the 1-D velocity model, we might expect the hypocentral depth to be poorly constrained. To fur-

ther examine the depth resolution we determined RMS error as a function of depth in the 0 to 30 km range with a spacing of 1 km, while keeping the epicentre fixed. The results are shown in Figure 8 and display a well-defined minimum at 14 km, suggesting that the assumption that the earthquake occurred at mid-crustal depths is reasonable.

A local Richter magnitude was determined from amplitude readings at seismograph stations in the distance range 80 to 230 km and at a range of azimuths. Maximum ground displacements and periods for simulated Wood-Anderson seismograms were measured on both horizontal components at three-component stations and the result averaged. The average magnitude based on readings from 9 stations was 4.7 ML.

Source Mechanism

A source mechanism for the earthquake was determined using two different methods: BGS calculated a focal mechanism analysis based on first motion polarities from locally recorded data within the UK; secondly, the Swiss Seismological Service, determined a moment tensor solution, based on waveform inversion of regional broadband recordings in the UK and other European countries (Bernardi et al., 2002). For the first-motion method, fifty-seven P-wave polarities were picked from vertical component recordings at local seismograph stations at a wide range of azimuths. The grid search method of Snoke et al. (1984) was then used to determine the best-fitting fault plane solutions, with a grid spacing of 2°. The 1-D velocity model and a fixed source depth of 14 km were used to determine takeoff angles. Thirty-four possible solutions were found to fit the observed polarity data which all showed very similar fault motion. A mean solution was then determined from the possible solutions. The regional moment tensor analysis provides a source solution that explains the observed seismograms for long-period waves with minimal error (Nabelek and Xia, 1995). The source mechanisms given by the two different methods are shown in Figure 9. Both solutions are very similar and show near vertical strike-slip faults strik-

ing either north south or east west, with a small thrust component. However, the dip of the two faults is slightly different. The first motion polarities show either left lateral strike slip motion on a north south fault, dipping to the east or right lateral strike slip motion on an east west fault dipping to the north. The moment tensor solution shows either left lateral strike slip motion on a north south fault, dipping to the west or right lateral strike slip motion on an east west fault dipping to the south. The P-axis orientations given by the two methods are also very similar, with the first motion polarities giving a P-axis azimuth and plunge of 320° and 1°, respectively, and the moment tensor inversion giving a P-axis azimuth and plunge of 324° and 4°, respectively. These directions agree well with the regional tectonic model, which predicts northwest compression due to the opening of the mid-Atlantic ridge and also with a best-fitting stress tensor obtained by Baptie (2002) from inversion of fault plane solutions for UK earthquakes. The T-axis orientations are 180° apart, reflecting the difference in dip.

The solutions seem quite stable to changes in focal depth and also near surface velocity, but slightly more sensitive to a change in the Moho depth. However, for example, a 32 km Moho, still results in similar solutions.

Waveform Modelling

Given the source mechanism discussed above and the 1-D velocity model used for earthquake location, we applied the discrete wave number method of Herrmann (1996) to generate synthetic seismograms at different azimuths and epicentral distances for a number of fixed source depths. Figure 10 shows observed and modelled seismograms in a short time window about the initial P-wave arrival for four source depths of 12, 14, 16 and 18 km at four stations in the distance range 80-230 km. The fault plane solution from first motion polarities was used as the source mechanism. A band pass filter of 1-4 Hz has been applied to the data. Visual comparison of the observed and modelled data shows that the models accurately capture many of the key characteristics of the observed

data. For example, the synthetics for station WOL, Figure 10 (c), with source depth 14 km, shows the initial low amplitude P-wave arrival followed by two higher amplitude phases, similar to those observed. Similarly, the 14 km source depth model at station AEU, Figure 10 (d), shows a low amplitude P-wave followed by three later phases, also observed in the data. The best match for the observed data at stations HBL2 and KEY2, Figure 10 (a) and (b), is given by source depths of 12 km and 16 km respectively. This highlights the degree of non-uniqueness in modelling high-frequency waveforms in the presence of uncertainties in the velocity model.

Figure 11 shows observed (black) and modelled (red) seismograms for five stations in the 80 to 150 km range over a slightly larger time window. Figure 12 shows similar observed and modelled seismograms for more distant stations in the 200-300 km range. In both cases the synthetic seismograms were generated using the method of Herrmann (1996) and a source depth of 14 km. The synthetics capture many of the features of the observations, for example, the modelled P- and S- waves at stations HBL2 and KEY2 are reasonable in terms of both arrival time and relative amplitude. Goodness of fit begins to decrease with distance, which may be a consequence of lateral variability in structure. However, we conclude that the 14 km source depth provides a good overall match for the observed waveforms, and qualitative evidence that the earthquake did occur at mid-crustal depth.

A Comparison of Aftershocks with Main Event

The Dudley main shock was followed by two aftershocks that were also recorded on the BGS seismic network. The earthquakes occurred on 23 September at 03:32 and 24 September at 09:29, with magnitudes 2.7 ML and 1.2 ML, respectively. Accurate P-wave arrival times were identified on stations within 116 km from the epicentre location of the main-shock for the three events in order to resolve the relative location of the three events. Relative time differences between the stations were generally of the order of 0.1 seconds and did not reveal

any conclusions on the relative locations since the observed differences were of the same size as the error in phase reading. In a more formal approach, the three events were jointly located using the program VELEST (Kissling et al., 1994). The results (Table 2) show that the two aftershocks were located within the error ellipsoid (90% confidence) of the main-shock, however, the relative differences possibly only reflect the uncertainties in the phase identification.

Detailed inspection of waveform signals from the first aftershock shows a small initial arrival that precedes the larger second arrival by 0.30 seconds (Figure 13). The first (P1) and second waveform signals (P2) appear to be nearly identical and are separated with a constant offset for various stations. This suggests that there were two events, the first and smaller event possibly initiating the rupture was followed by a larger event, which mostly contributed to the signal recorded as the first aftershock. The similarity in the waveform signals, which can only be observed for 0.3 seconds, suggests that the two events were practically identical with respect to both hypocentre location and mechanism.

Comparing signals from the main-shock and the first aftershock on a number of stations (Figure 14) reveals a high degree of similarity, both with respect to phase arrival times as well as amplitude ratios between the various phases. The similarity in arrival times between the two events at a number of stations indicates that they are co-located. The match of amplitude ratios of seismic phases between events can be explained by a similar source mechanism. Unfortunately the number of stations suited for comparison of the main- and first aftershock is rather limited, since data for the main-shock at shorter distances on normal gain instruments are clipped. At the same time, since the aftershock is of much smaller size, the strong motion or low-gain instruments at shorter distances did not record the signals with sufficient amplitude for comparison, while at larger distances the signal to noise ratio was reduced compared to the larger main-shock. However, from the limited number of stations available for this comparison, it seems likely that both main-shock and aftershock had a similar source mechanism.

Comparison of waveform signals between the two aftershocks from a number of

stations also showed strong similarities (Figure 15). It therefore seems likely that both events are very similar with respect to hypocentre location and mechanism. A perfect match between the two aftershocks cannot be expected due to the complexity of the first aftershock as it is preceded by a smaller event.

The source mechanism of the aftershocks could not be obtained directly due to the complexities of the first and the small size of the second, which did not allow the determination of a sufficient number of polarities. However, the comparison of waveform signals indicates that the three events probably had a similar or even identical mechanism. The few polarity readings that could be made for the first aftershock do not contradict this suggestion.

Peak ground motion

Figure 16 shows the decay in observed peak vertical ground acceleration (PVGA) with hypocentral distance for the main shock. Hypocentral distance, r_{hyp}, was calculated using a source depth of 14 km. Because deconvolving the instrument response amplifies noise outside the pass-band of the recording instrument, all signals were filtered between 1 and 25 Hz before measurements were made. PVGA decays exponentially from $15.3 cm/s^2$ at station KEY2, at Keyworth, near Nottingham (r_{hyp} = 85 km), to $0.05 cm/s^2$ at station JRS at Maison St. Louis in Jersey (r_{hyp}=371 km). The highest acceleration was observed at station KEY2 (r_{hyp} = 85 km) and this is the only station where the peak acceleration is observed in the *P*-wave. The general scatter in the observed peak ground motion values is primarily a result of attenuation, both along the path and at the station.

There are 47 observations of PVGA for the largest aftershock (magnitude 2.7 ML), at distances between 64 km and 346 km from the epicentre (Figure 17). These observations exhibit more scatter than for the main shock, because the corner frequency is higher and the signal more sensitive to variations in the quality factor Q and the parameter κ describing near-surface attenuation.

Figure 18 shows the observed peak horizontal ground acceleration (PHGA) for the main shock. PHGA is defined as the maximum of the peak accelerations observed on the radial and transverse components. PHGA decays exponentially with distance from $15.6cm/s^2$ at KEY2 to $0.02cm/s^2$ at station MCD, Coleburn Distillery, Moray ($r_{hyp} = 568$ km). Again the highest on-scale ground acceleration within the frequency band is observed in the P-wave at KEY2, $15.6cm/s^2$. However, the peak acceleration associated with the shear wave at this station is $6.3cm/s^2$, a value more consistent with the other observations. The average ratio of PHGA to PVGA is 1.71 ± 0.26. This is comparable to the ratio of 1.6 ± 0.6 found for firm soil and bedrock sites in Canada (Cassidy et al. (1997)).

The PHGA predicted using five empirical relations, considered applicable in the UK, are also shown in Figure 18. These relations all over-predict the observed PHGA. However, it is now well recognised that such ground motion predictions, which are not UK specific and are often derived using data from more than one tectonic region, are a systematic source of over-conservatism in site-specific hazard assessment in the UK (Aspinall et al., 2002).

Predicting Peak Ground Acceleration Using Random Vibration Theory

An attenuation relation that is specific to the UK has yet to be developed due to the lack of data, particularly from larger earthquakes. However, in low seismicity regions, the stochastic method (Boore, 1983) can be used to synthesise ground motion datasets from which attenuation relations can be derived. Such an approach has proved effective in areas such as Eastern North America (Toro et al., 1997).

Here, PHGA is simulated using the results of Random Vibration Theory (RVT) (Vanmarcke and Lai, 1980). Unlike Boore's stochastic method, which simulates the acceleration time history to determine PHGA, RVT permits PHGA to be calculated directly from the theoretical acceleration spectrum. Boore (1983)

shows that the results obtained using the RVT approach are comparable to the peak motions estimated from simulated time series.

Provided that the seismic moment M_0 and stress drop $\Delta\sigma$ are known, PHGA can be calculated from the theoretical acceleration spectrum using the results of RVT (Vanmarcke and Lai, 1980). Using the first (mean), second (variance) and fourth statistical moments of the energy density spectrum, the spectral bandwidth, rms acceleration (a_{rms}) and predominant frequency may be found. Maximum acceleration can then be determined from a_{rms} and the expected number of acceleration extrema in a specified time interval (assuming a stationary time series with uncorrelated peaks).

The RVT method is used here to estimate PHGA over a range of distances ($5 < r_{hyp} < 600km$). Hypocentral distance is used here because the extent of the rupture is small ($R \simeq 1km$), and using epicentral distance or the Joyner-Boore distance may cause ground motion to be overestimated, particularly in the near-field.

We use the method of Ottemoller and Haskov (2003) to automatically determine seismic moment, M_0, and corner frequency, f_c, from the observed vertical displacement spectrum of L_g waves. Automated processing, which determines the source parameters by a grid-search, is considered to be more objective than manual determination from the source spectra. The L_g wave time window was defined by group velocities between 3.0 and 3.6 km/s.

The closest unsaturated records for the main shock and the largest aftershock are from epicentral distances of 80 km and 64 km, respectively. The initial data set for each earthquake included all on-scale records where L_g was clearly observed. Those records which did not meet the prescribed signal-to-noise criteria used by the program, over a wide enough range of frequencies for f_c to be determined reliably, or those where the spectrum deviated significantly from the expected ω^2 model, were removed from the final data set used to calculate the average source parameters.

Observed spectra were corrected for geometrical spreading, path dependent and

near-surface attenuation, source radiation and free-surface effects. The quality factor for the path dependent anelastic attenuation $Q(f) = 440f^{0.7}$, determined for Norway, was used (Kvamme et al. (1995)). The near-surface attenuation is assumed to be of the form $D(f) = -exp(\pi\kappa f)$, proposed by Anderson and Hough (1984). We assume a value for κ of 0.02 at all stations.

The results of the spectral analysis for the mainshock and aftershock respectively are given in Tables 3 and 4. We conclude from these results that the $Q(f)$ estimate is appropriate because the low frequency spectral level, Ω_0, does not appear to be dependent on distance. The corner frequency f_c is difficult to constrain (1.19 $\pm$ 0.56 Hz), and combined with variations in Ω_0, leads to large uncertainties in the Brune stress drop (11.82 $\pm$ 12.04 bar) for the main shock. The average moment magnitude M_W is 4.2 $\pm$ 0.13. For the largest aftershock, the standard deviation of the stress drop estimate is 91% of the average value (22.04 $\pm$ 20.07 bar). These uncertainties reflect the station-to-station variability of the corner frequency.

In Figure 19, observed PHGA from the mainshock is compared with the theoretical values calculated using RVT. Predicted PHGA calculated using a model which incorporates the average values of M_W and $\Delta\sigma$ in Table 3, defines the lower bound on observed ground motion. Given the simple near-surface attenuation model that has been used, the misfit between the observed and synthetic data is unsurprising. When PHGA is calculated using the M_W and $\Delta\sigma$ estimates for each station (where they are available), closer agreement between the observed and predicted PHGA values is achieved. This is because the individual stress drop estimates compensate for the shortcomings in our estimate of κ at each station.

We also estimate ground motion using the upper standard deviation on M_W and $\Delta\sigma$. Although PHGA calculated with this model follows the observed data more closely, the four closest observations (from strong motion instruments) are underestimated. Using this model, we estimate that PHGA at the epicentre was at least $19cm/s^2$ (0.02 g). Without more data, this value should be treated as the lower limit on PHGA at the epicentre.

For the aftershock (Figure 20), there is better agreement between the observed and synthetic PHGA values and the average model serves roughly as the upper bound on ground motion. Using the standard deviation on the mean values of M_W and $\Delta\sigma$, only two observations are underestimated by this model. If the quality of fit in the far-field can be assumed to be indicative of the suitability of the model for estimating PHGA in the near-field, we estimate that peak acceleration at the epicentre was of the order of $4.5cm/s^2$ (0.005 g).

Discussion

Instrumental data have been used to determine a hypocentre and source mechanism for the Dudley earthquake. The earthquake epicentre appears to be well constrained, with good azimuthal coverage, although the closest station is 58 km distant. Focal depth is less well constrained though the distribution of RMS errors with depth shows a clear minimum at 14 km. However both depth and mechanism depend on the seismic velocity model used to locate the earthquake and determine source takeoff angles, which can add to the uncertainty in both. In this case the velocity model is rather poorly known. Most of the published information on seismic velocity structure in the UK has been obtained from large-scale seismic refraction and wide-angle reflection surveys carried out by various institutes (Booth, 2001) and the 1-D models of seismic velocity as a function of depth used by BGS for earthquake location in the UK are derived from these studies. However, few refraction profiles have been carried out in central and southern England and the 1-D model derived for the Midland valley of Scotland has commonly been applied to this region. This model divides the crust into three main units, typically observed across the UK: a sedimentary overburden; a crystalline upper crust of deformed metamorphic and igneous rocks; and a lower crust. Previous results suggest that this is a reasonable approximation with earthquakes and other seismic events generally being located within a few kilometres of the area of peak intensity. However, no calibration studies have been undertaken for events in this region. Table 5 shows the dependence of hypocentre depth on the Moho depth for the Dudley earthquake.

The source depth could vary between 10-20 km depending on the Moho depth. The overall crustal thickness used in the 1-D model is 34 km. Chadwick and Pharaoh (1998) find a depth for the seismic reflection Moho in the Midlands of 32-34 km, though this is poorly constrained, and Tomlinson (2001) finds a crustal thickness of 34-36 km from teleseismic receiver functions determined at three-component stations within 62-80 km of the Dudley epicentre.

Two independent methods of determining the earthquake source mechanism both give very similar solutions, except for small variations in the direction of dip and sense of slip. The focal mechanism determined using first motion polarities is relatively insensitive to changes in focal depth and within the depth error of 3.7 km the mechanism remains unchanged, suggesting that this solution does not have a critical dependence on the velocity model and is reasonably robust. The moment tensor inversion showed that the event cannot be shallower than about 9 km, however, solutions of up to about 30 km would still match the observed data (pers. comm. Braunmiller, 2003). The calculated direction of maximum compressive stress also shows good agreement with the expected stress regime from first order plate motions and with the best-fitting stress tensor given by inversion of UK earthquake focal mechanisms.

Waveform modelling provides further support for a focal depth of 14 km, but again there is a strong dependency on the velocity model used to generate the synthetics. Lateral variation in structure is likely to cause significant variations in the observed seismograms both with distance and azimuth, therefore waveform modelling has to be used with caution as a quantitative tool to constrain source depth by modelling high frequency data.

The earthquake epicentre lies in a major zone of faulting associated with the Western Boundary Fault of the South Staffordshire Coalfield, an important basin-controlling normal fault with significant syndepositional throw. It seems likely that movement on a fault, or faults, associated with this zone could have caused the earthquake. The surface trace of the Western Boundary Fault passes to the west of Dudley and to the east of Stourbridge along a southerly or south-easterly trend (Figure 5) and the fault throws down Triassic rocks to the west

against older (Upper Carboniferous rocks) of the South Staffordshire Coalfield to the east. The epicentre was estimated at a depth of 14 km and about 1 km to the west of the Western Boundary Fault. The horizontal error in epicentre determination is of the order of 1-3 km, which means that several faults could have been the source of the event. The majority of the larger faults trend NE-SW, which may indicate that the north-south nodal plane is more likely to be the fault plane of the earthquake. The westward dip of the Western Boundary fault shows better agreement with the moment tensor solution than the solution from first motion polarities; however, it is unknown how the faults continue at depth. The mid-crustal depth of the earthquake implies that the fault zone extends from the surface to significant depths.

The similarity of the waveforms between the main shock and the aftershocks suggests that they all occurred within a small source volume, of the order of a few hundred metres. In addition, the complex nature of the waveform for the first and largest aftershock suggests that a two-stage rupture may have taken place, with a smaller rupture initiating further slip possibly along the same fault.

The average moment magnitude of 4.2 M_W, determined from the source spectra, is in keeping with the value of 4.3 M_W obtained by the moment tensor inversion of the Swiss Seismological Service. The Brune stress drop parameter, $\Delta\sigma$, has a large uncertainty associated with it, that reflects station-to-station variability of the corner frequency measurement. This variability could to some extent result from the assumed value for the near-surface attenuation parameter, κ, of 0.02 at all stations.

Using the stochastic method, it is possible to achieve a reasonably good fit between the observed and theoretical PHGA values for the Dudley mainshock and aftershock using a simple attenuation model. For future studies in the UK, it is likely that the quality of the fit could be further improved if only the records from stations sited on hard rock were included. However, with the lack of PHGA data in the UK, it would be preferable for κ to be reliably defined at each station rather than further reducing the size of the dataset.

Conclusions

- The source depth for the earthquake, constrained by waveform modelling, shows that the earthquake occurred in the mid-crust.
- The source mechanism suggests strike-slip faulting along a near-vertical fault-plane that strikes north-south. This observation is in agreement with both the surface expressions of faulting in the area and also with the expected regional stress tensor from first order plate motions.
- It seems likely that the earthquake can be associated with the Western Boundary fault of the South Staffordshire Coalfield, a significant fault in the region.
- The main shock and the aftershocks all occurred within a small source volume, of the order of a few hundred metres and had similar source mechanisms.
- The rupture for the largest aftershock probably comprised two stages with a smaller rupture initiating further slip. It is not possible to say if this is also the case for the mainshock.
- The observed peak ground acceleration is considerably less than that predicted by empirical relations, which are currently used in the UK. A better match for the observed ground motions is achieved using a stochastic approach to model both the mainshock and the first aftershock.

Acknowledgements

The authors thank Jochen Braunmiller of the Swiss Seismological Service for providing the moment tensor solution and discussions on the uncertainties. Additional data used to locate the earthquake and determine a fault plane solution was provided by Keele University, AWE Blacknest (station WOL), IRIS/IDA (station ESK) and GEOFON (station DSB). Project IDA is a global network of broadband and very long period seismometers operated by the Institute of

Geophysics and Planetary Physics, Scripps Institution of Oceanography, University of California, San Diego. The GEOFON network is funded and operated by GFZ Potsdam, Germany, in co-operation with almost 50 institutions world-wide. Julian Bukits provided the macroseismic information and also assisted with diagrams. David Booth and Alice Walker are also thanked for their comments and suggestions. This work is published with the approval of the Executive Director of the British Geological Survey (NERC).

References

Anderson, J., and Hough, S., 1984, A model for the shape of the Fourier amplitude spectrum of acceleration at high frequencies: Bull. Seis. Soc. Am., **74**, 1969–1993.

Aspinall, W., Mallard, D., Skipp, B., and Woo, G., 2002, On scatter and conservatism in seismic attenuation relations: 12th European Conference on Earthquake Engineering.

Assumpção, M., and Bamford, D., 1978, LISPB V. Studies of crustal shear waves: Geophys. J.R. astr. Soc., **54**, 61–73.

Bamford, D., Nunn, K., Prodehl, C., and Jacob, B., 1978, LISPB-IV. crustal structure of Northern Britain.: Geophys. J.R. astr. Soc., **54**, 43–60.

Baptie, B., State of stress in the UK from observations of local seismicity:, In Preparation, 2002.

Bernardi, F., Braunmiller, J., Kradolfer, U., and Giardini, D., 2002, Fully automated regional moment tensor inversion in the European Mediterranean area: European Seismological Commission, XXVIII General Assembly, Genoa, 215.

Boore, D., 1983, Stochastic simulation of high-frequency ground motions based on seismological models of radiated spectra: Bull. Seis. Soc. Am., **73**, 1865–1894.

Booth, D., Review of velocity structure in the UK and adjacent areas:, Technical Report CR/01/79, British Geological Survey, 2001.

Burton, P., Musson, R., and Neilson, G., Macroseismic report on historical British earthquakes IV: Lancashire and Yorkshire:, Global Seismology 219, British Geological Survey, 1984.

Cassidy, J., Rogers, G., and Wiechert, D., 1997, Soil response on the Fraser Delta to the MW=5.1 Duvall, Washington, earthquake: Bull. Seis. Soc. Am., **87**, no. 5, 1354–1362.

Chadwick, R., and Pharaoh, T., 1998, The seismic reflection Moho beneath the United Kingdom and adjacent areas: Tectonophysics, **299**, 255–279.

Herrmann, R. **Computer Programs in Seismology**. Saint Louis University, 1996.

Kissling, E., Ellsworth, W., Eberhart-Phillips, D., and Kradolfer, U., 1994, Initial reference model in local earthquake tomography: J. Geophys. Res, **99**, no. 19, 19635–19646.

Kvamme, L., Hansen, R., and Bungum, H., 1995, Seismic-source and wave-propagation effects on Lg waves in Scandinavia: Geophys. J. Int., **120**, 525–536.

Lienert, B., Berg, E., and Frazer, L., 1988, Hypocenter, an earthquake location method using centered, scaled and adaptively least squares: Bull. Seis. Soc. Am., **76**, 771–783.

Main, I., Irving, D., Musson, R., and Reading, A., 1999, Constraints on the frequency magnitude relation and maximum magnitudes in the UK from observed seismicity and glacio-isostatic recovery rates.: Geophys. J. Int., **137**, 535–550.

Musson, R., Neilson, G., and Burton, P., Macroseismic report on historical British earthquakes XII: North Wales and Irish Sea:, Global Seismology 28, British Geological Survey, 1984.

Musson, R., A catalogue of British earthquakes:, Technical Report WL/94/04, British Geological Survey, 1994.

Nabelek, J., and Xia, G., 1995, Moment tensor analysis using regional data: application to the 25 March, 1993, Scotts Mills, Oregon, earthquake: Geophys. Res. Lett., **22**, 13–16.

Neilson, G., Musson, R., and Burton, P., Macroseismic report on historical British earthquakes XI: 1931 June 7 North Sea:, Global Seismology 280, British Geological Survey, 1986.

Ottemoller, L., and Haskov, J., 2003, Moment magnitude determination for local and regional earthquakes based on source spectra: Bull. Seism. Soc. Am.

Pharaoh, T., Molyneux, S., Merriman, R., Lee, M., and Verniers, J., 1993, The Caledonides of the Anglo-Brabant Massif reviewed: Geol. Mag., **130**, no. 5, 561–562.

Powell, J., Glover, B., and Waters, C. N., A geological background for planning and development in the Black Country:, Technical Report WA/92/33, British Geological Survey, 1992.

Ritchie, M., Musson, R., and Woodcock, N., 1990, The Bishop's Castle earthquake of 2 April 1990: Terra Nova, **2**, 390–400.

Simpson, B., A Bulletin of British Earthquakes 2002:, Technical Report WL/02/01, British Geological Survey, 2002.

Snoke, J., Munsey, J., Teague, A., and Bollinger, G., 1984, A program for focal mechanism determination by combined use of polarity and SV-P amplitude ratio data: Earthquake Notes, **55**, 3–15.

Tomlinson, J., 2001, A teleseismic receiver function study of the crustal structure of the British Isles: European Geophysical Society, 26th General Assembly, Nice, France, Geophysical Research Abstracts.

Toro, G., Abrahamson, N., and Schneider, J., 1997, Model of strong ground motions from earthquakes in Central and Eastern North America: best estimates and uncertainties.: Seism. Res. Lett., **68**, no. 1, 41–73.

Vanmarcke, E., and Lai, S.-S., 1980, Strong motion duration and RMS amplitude of earthquake records: Bull. Seis. Soc. Am., **70**, no. 4, 1293–1307.

Depth to top of layer (km)	P-wave velocity (km/s)	V_p/V_s
0.00	4.00	1.73
2.52	5.90	
7.55	6.45	
18.87	7.00	
34.15	8.00	

Table 1: Crustal Velocity model used in earthquake location.

Date	Origin time	Latitude	Longitude	Depth (km)	No. of stations	Rms (seconds)
2002/09/22	23:53:14.6	52.528	2.139	15.7	9	0.064
2002/09/23	03:32:15.9	52.526	2.145	13.1	9	0.055
2002/09/24	09:29:19.2	52.533	2.156	14.2	4	0.054

Table 2: Results of joint hypocentre determination of the mainshock and its' two aftershocks.

Station	R (km)	$\log M_0$	$\delta\sigma(bars)$	Ω_0	$f_c(Hz)$	M_W
WOL	147	15.4	21.2	4.2	1.53	4.2
XDE	238	15.2	16.5	3.9	1.63	4.1
BBO	257	15.3	13.1	3.9	1.47	4.1
BDL	259	15.5	23.8	4.1	1.54	4.3
BTA	267	15.6	13.7	4.2	1.18	4.3
GCD	286	15.2	26.3	3.8	1.96	4.1
BHH	294	15.3	20.8	3.9	1.65	4.2
BBH	295	15.7	7.7	4.2	0.91	4.4
ECK	302	15.2	32.7	3.8	2.13	4.1
GMM	316	14.9	15.5	3.5	2.04	3.9
ESK (B)	318	15.3	4.0	3.9	0.95	4.2
ESK (S)	318	15.2	12.1	3.8	1.48	4.1
CCA	335	15.3	33.2	3.8	1.98	4.1
CGH	344	15.3	45.1	3.8	2.25	4.1
PCA	379	15.3	2.7	3.8	0.85	4.1
ESY	379	15.5	4.3	4.0	0.85	4.3
EDI	384	15.4	4.7	3.9	0.94	4.2
PCO	405	15.6	1.0	4.0	0.51	4.3
PMS	406	15.7	2.3	4.2	0.59	4.4
EAB	431	15.4	2.8	3.8	0.82	4.2
EDU	451	15.7	1.8	4.2	0.54	4.4
EDR	489	15.5	4.6	3.9	0.86	4.3
MDO	564	15.1	3.6	3.5	1.08	4.0
MCD	567	15.8	1.5	4.1	0.49	4.4
MVH	614	15.5	1.7	3.9	0.61	4.3
RRR	636	15.4	1.0	3.8	0.55	4.2
RTO	699	15.4	1.5	3.7	0.63	4.2
Average		15.40	11.82	3.91	1.19	4.20
σ		0.21	12.04	0.19	0.56	0.13

Table 3: Source parameters for the mainshock (4.7 ML) determined automatically from vertical L_g-wave spectra.

Station	R (km)	$\log M_0$	$\Delta\sigma(bar\,s)$	Ω_0	$f_c(Hz)$	M_W
SSW	64	12.8	20.9	1.9	11.37	2.5
KTG	119	13.4	62.5	2.3	10.06	2.9
WFB	129	13.0	17.7	1.9	9.05	2.6
WPM	144	13.2	3.5	2.0	4.73	2.7
YLL	152	13.1	9.4	1.9	7.15	2.7
YRE	162	13.2	9.0	1.9	6.6	2.7
YRH	171	13.0	31.3	1.8	11.19	2.6
Average		13.10	22.04	1.96	8.59	2.67
σ		0.19	20.07	0.16	2.51	0.13

Table 4: Source parameters for the largest aftershock (2.7 ML) determined automatically from vertical Lg-wave spectra.

Moho Depth (km)	Source Depth (km)	RMS
30	8.4	0.31
31	9.4	0.31
32	10.7	0.31
33	11.5	0.31
34	12.9	0.33
35	19.2	0.37
36	20.8	0.37

Table 5: Dependency of source depth with Moho depth.

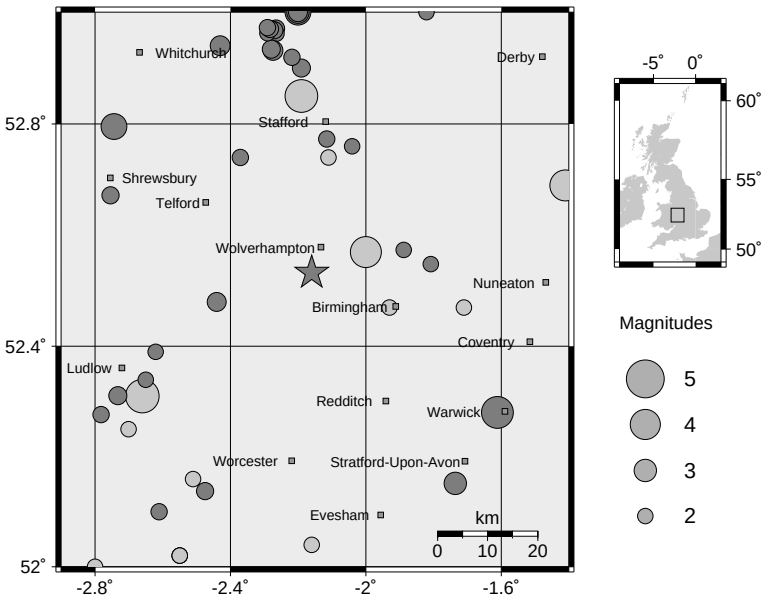

Figure 1: Instrumental (dark circles) and historical (light circles) seismicity of the West Midlands from 1768 to the present, in a 100 km square centred on the 2002 epicentre, marked by the star.

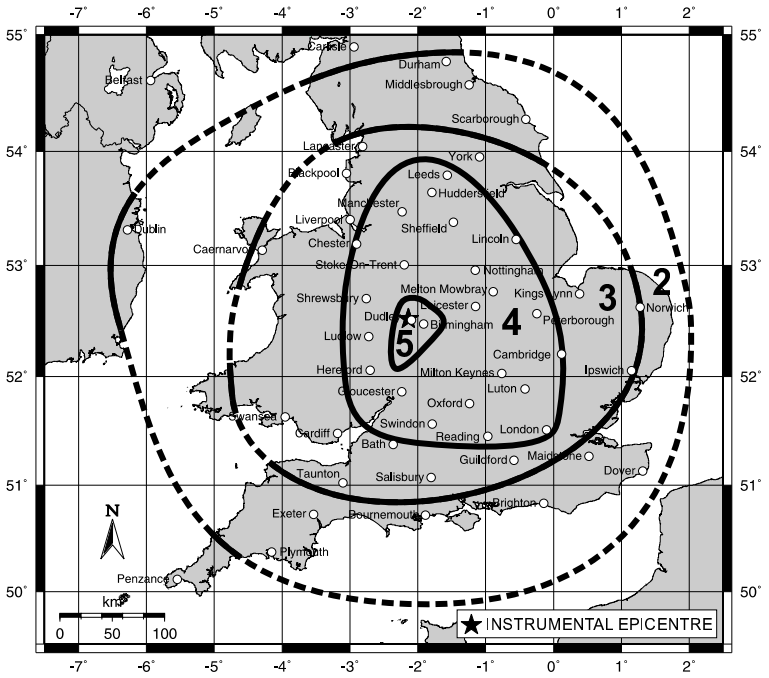

Figure 2: Macroseismic intensity map for the Dudley earthquake. Isoseismal contours denote EMS Intensities. The 2002 epicentre is marked by a star.

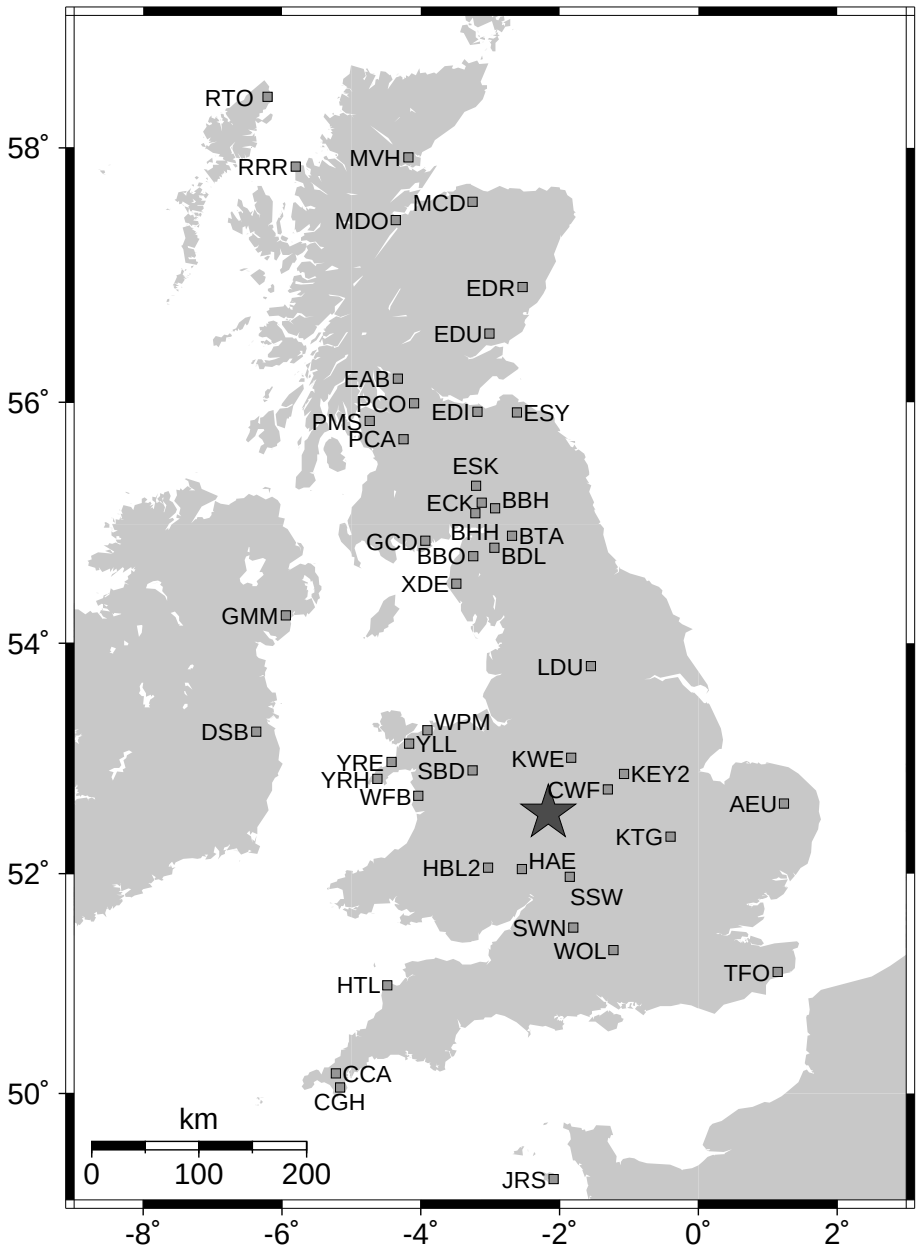

Figure 3: Seismograph stations used in subsequent analyses and mentioned specifically in the text. The 2002 epicentre is marked by a star.

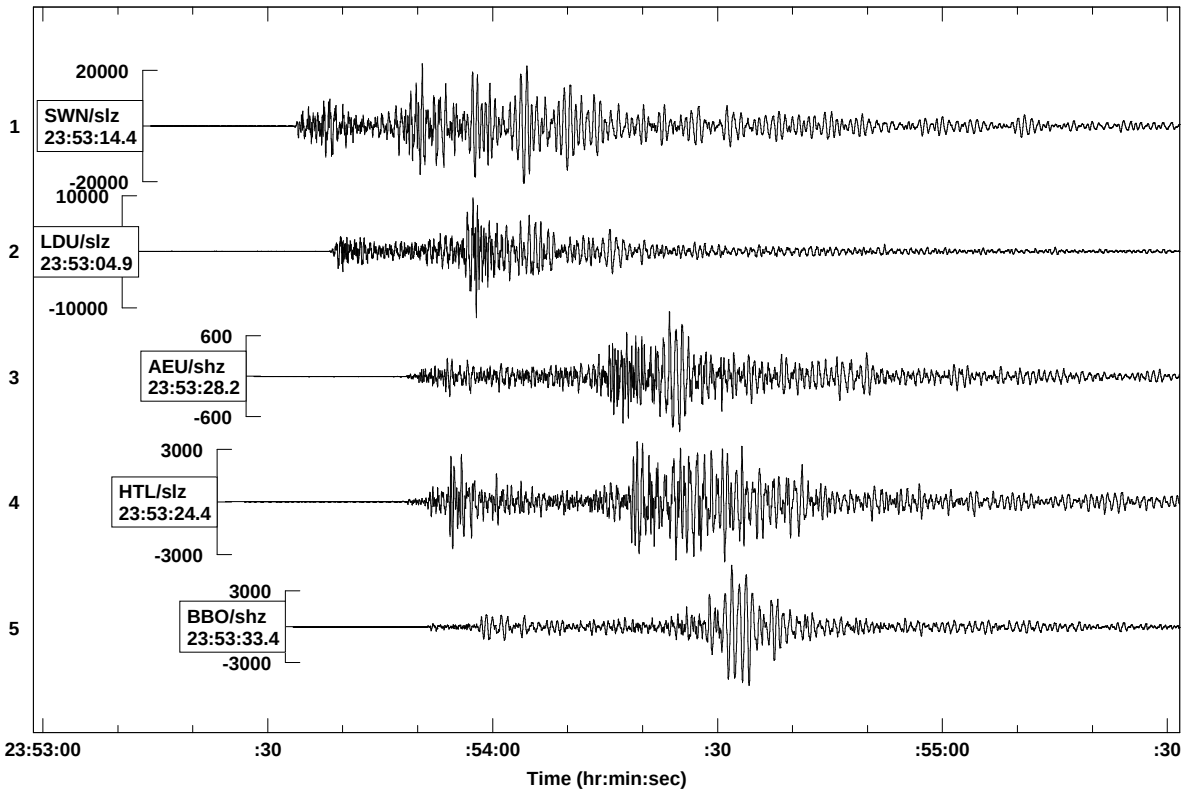

Figure 4: Seismograms of the vertical component of ground displacement at five low gain stations in the UK at epicentral distances ranging from 100 to 250 km.

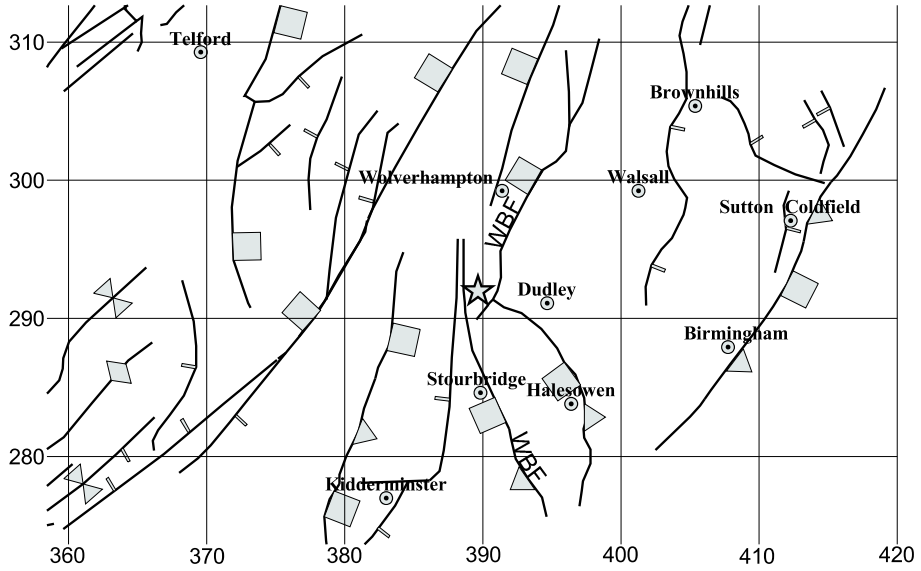

Figure 5: Surface trends of the principal faults in the West Midlands. Normal faults are denoted by a square on the downthrown side, while reverse faults are denoted by a barb on the upthrown side. The Western Boundary Fault is denoted by WBF.

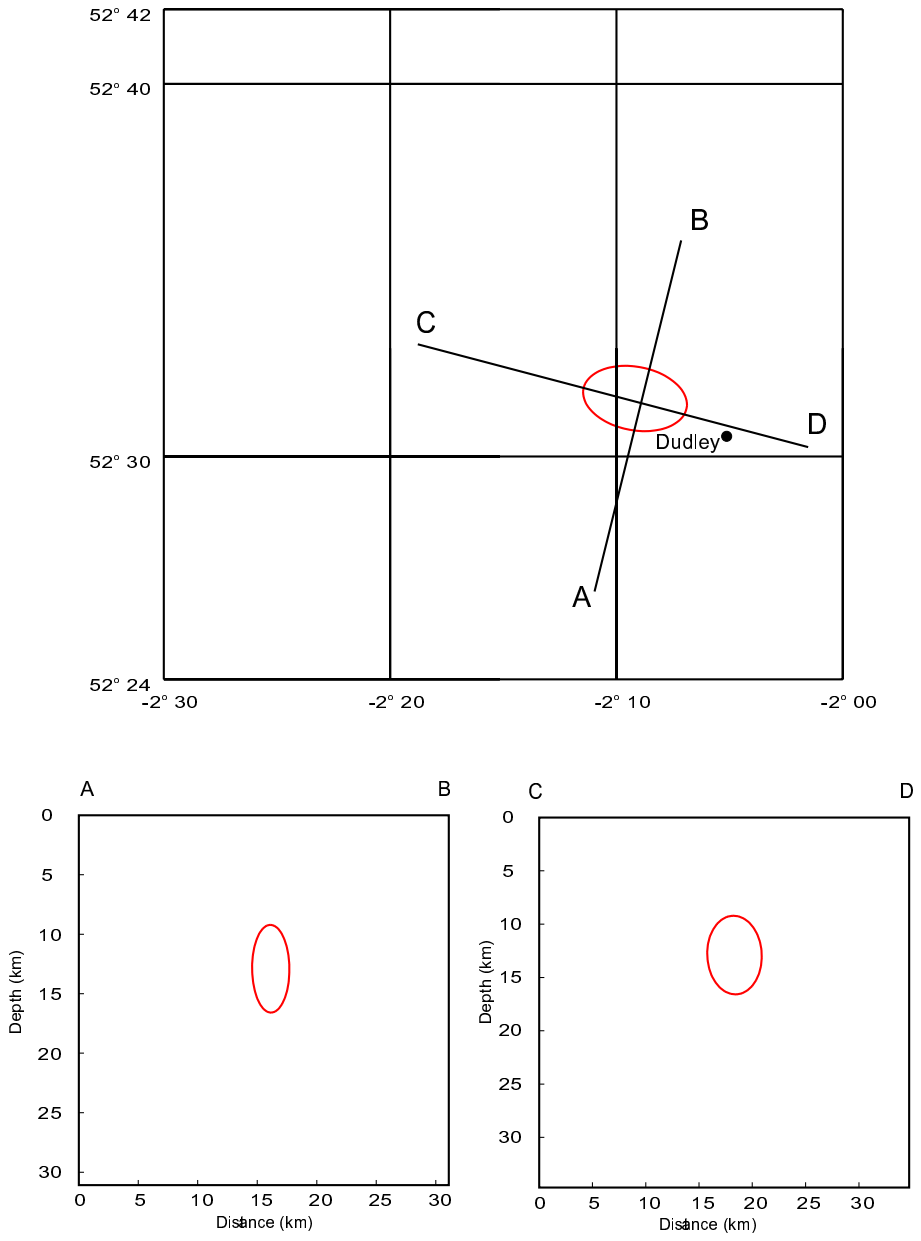

Figure 6: Horizontal and vertical projections of the 90% confidence ellipsoid for the calculated hypocentre of the Dudley earthquake.

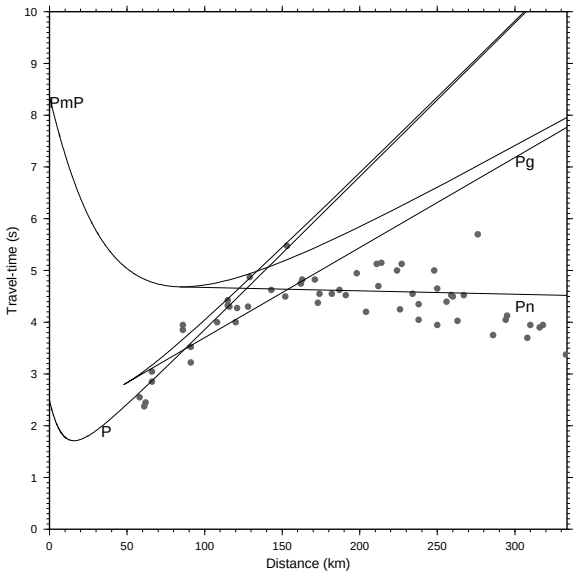

Figure 7: Reduced P-wave travel times for the Dudley earthquake as a function of epicentral distance for both observed (grey circles) and modelled data. Theoretical P-wave travel-time curves for primary crustal phases are determined for the 1-D velocity model used to locate the earthquake. The data have been reduced using a reduction velocity of 8 km/s.

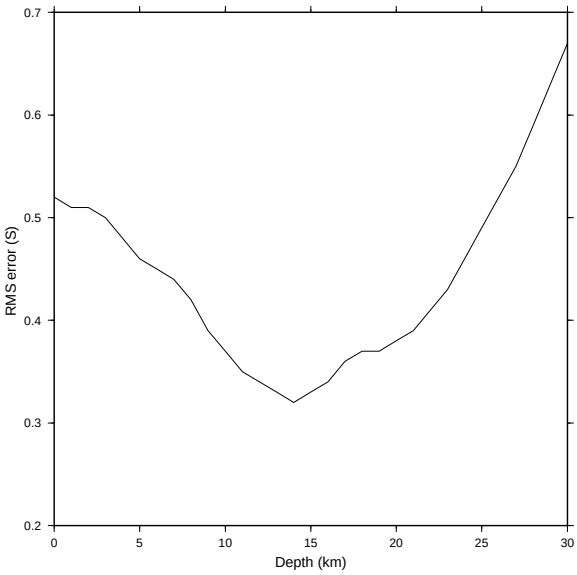

Figure 8: RMS error in earthquake location as a function of depth.

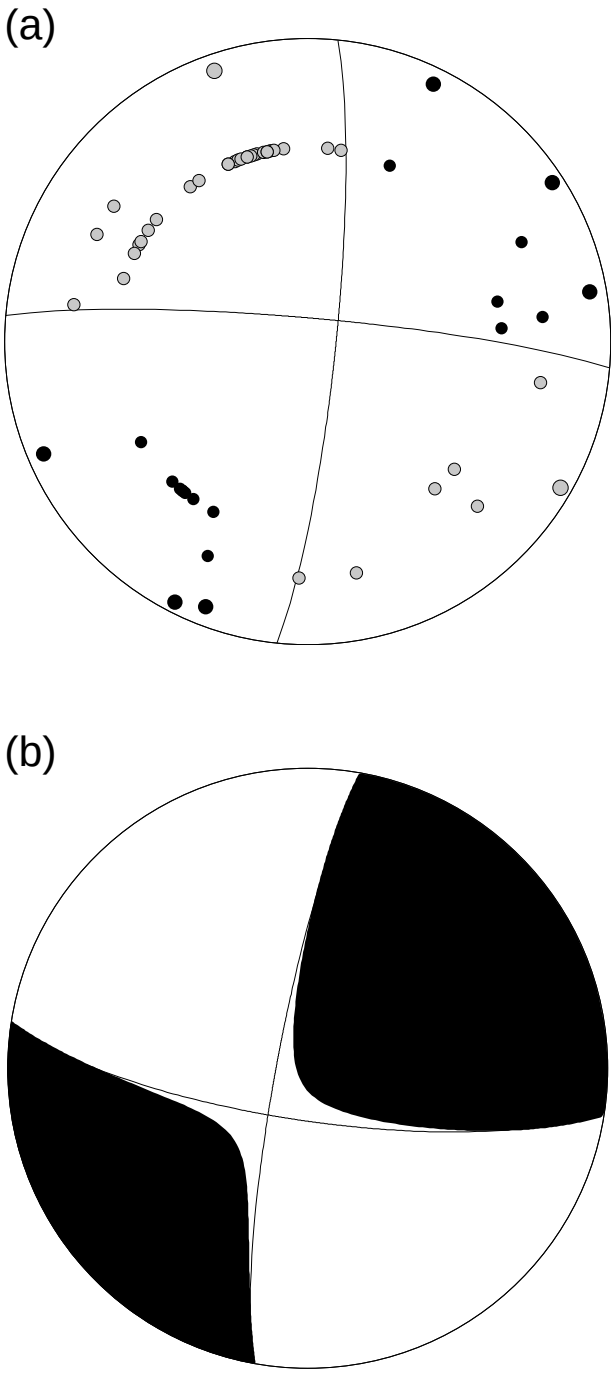

Figure 9: Source mechanisms determined for the Dudley earthquake using (a) first motion polarities from local recordings and (b) moment tensor inversion of regional broadband waveforms. The best-fitting double-couple solution is given by the black lines.

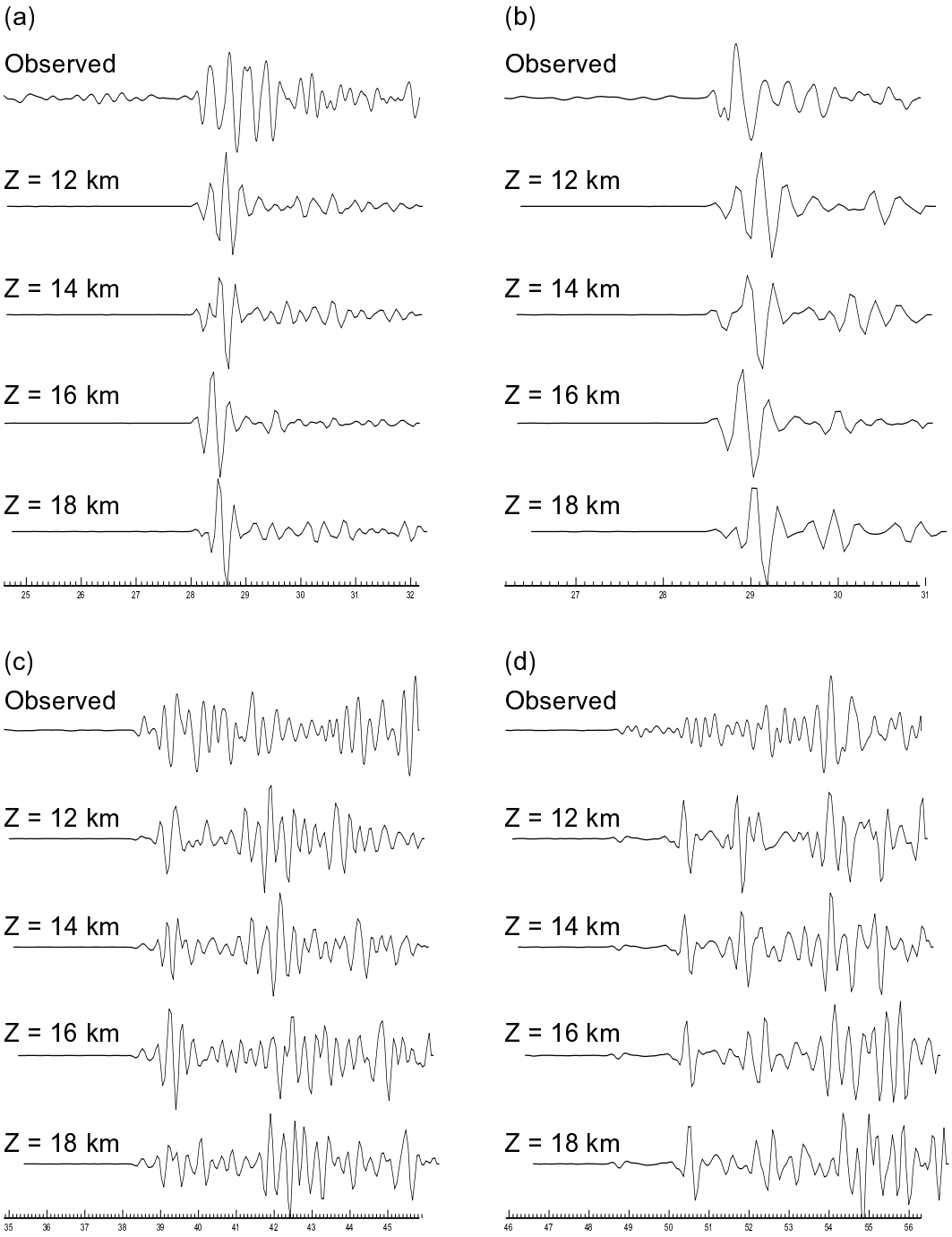

Figure 10: Observed and modelled seismograms for four source depths of 12, 14, 16 and 18 km at stations (a) HBL2, epicentral distance 80 km, (b) KEY2, epicentral distance 82 km, (c) WOL, epicentral distance 149 km, (d) AEU, epicentral distance 230 km.

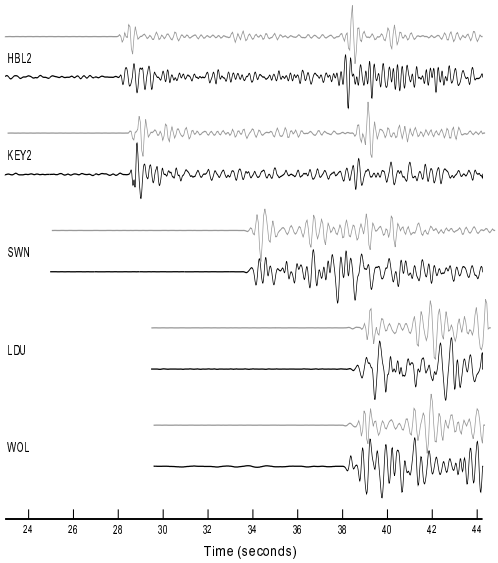

Figure 11: Observed (black) and modelled (grey) seismograms for stations HBL2 (80 km), KEY2 (82 km), SWN (115 km), LDU (148 km) and WOL (149 km). The synthetics were generated using a source depth of 14 km.

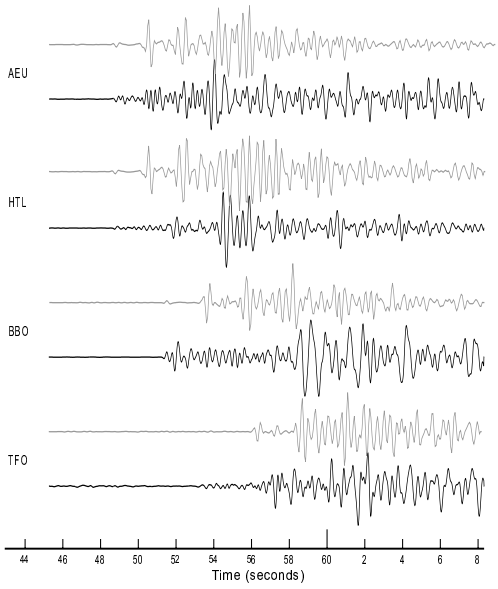

Figure 12: Observed (black) and modelled (grey) seismograms for stations AEU (230 km), HTL (234 km), BBO (256 km), and TFO (276 km). The synthetics were generated using a source depth of 14 km.

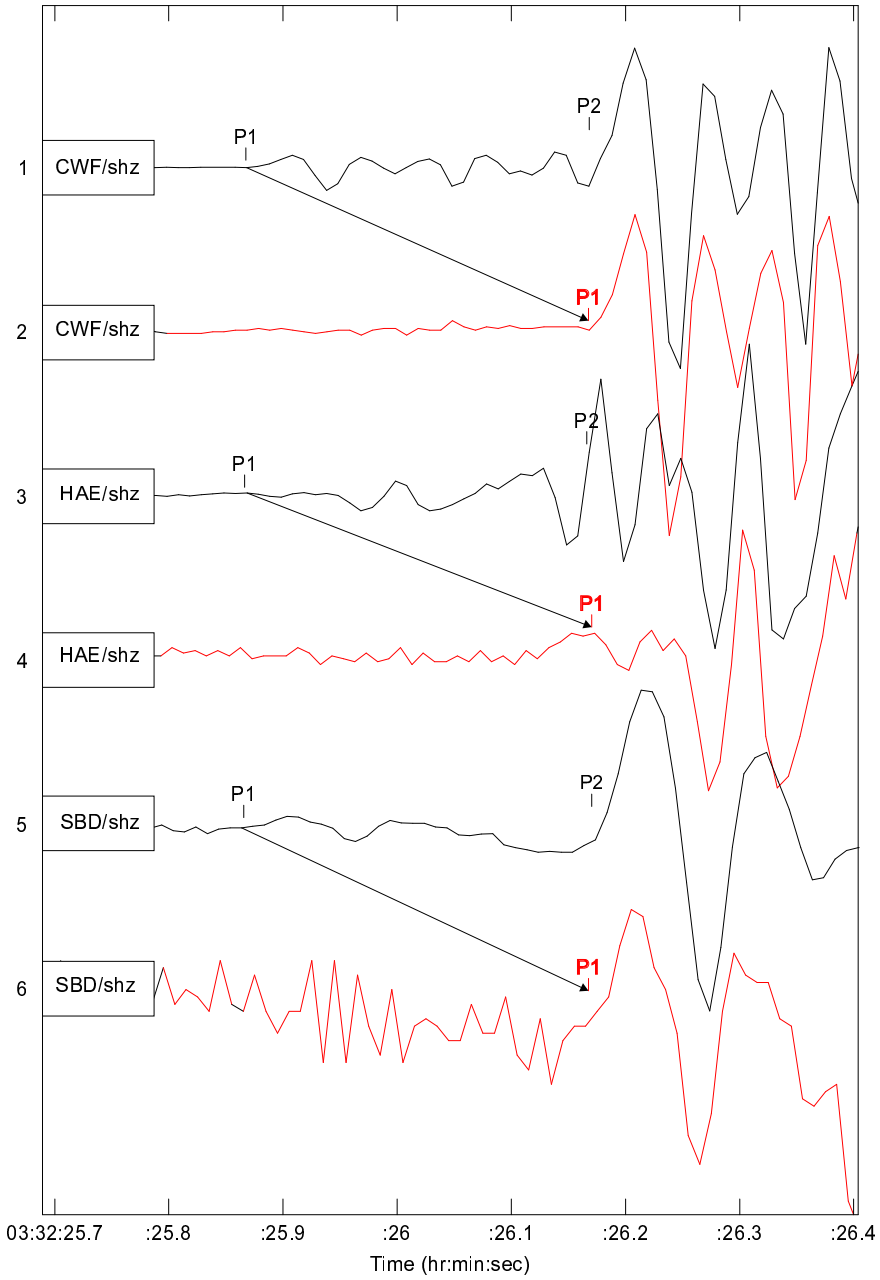

Figure 13: Waveforms from the first aftershock at 03:32 UTC on 23 September. The red traces show the precursory signal aligned in time with the larger arrival and the similarity of the signals at the three stations CWF, HAE and SBD.

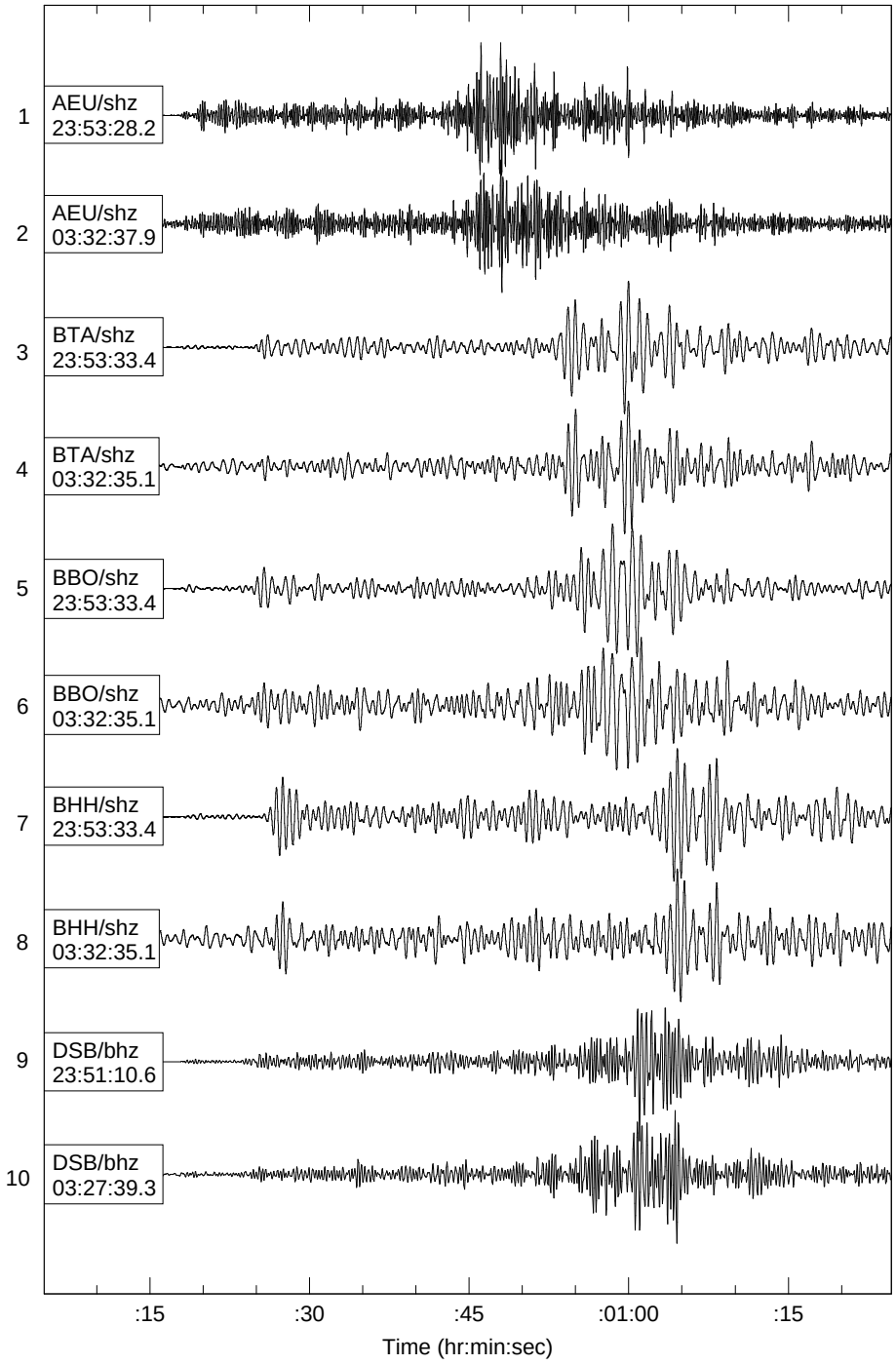

Figure 14: A comparison of the waveforms from the mainshock and the first aftershock at 03:32 UTC on 23 September.

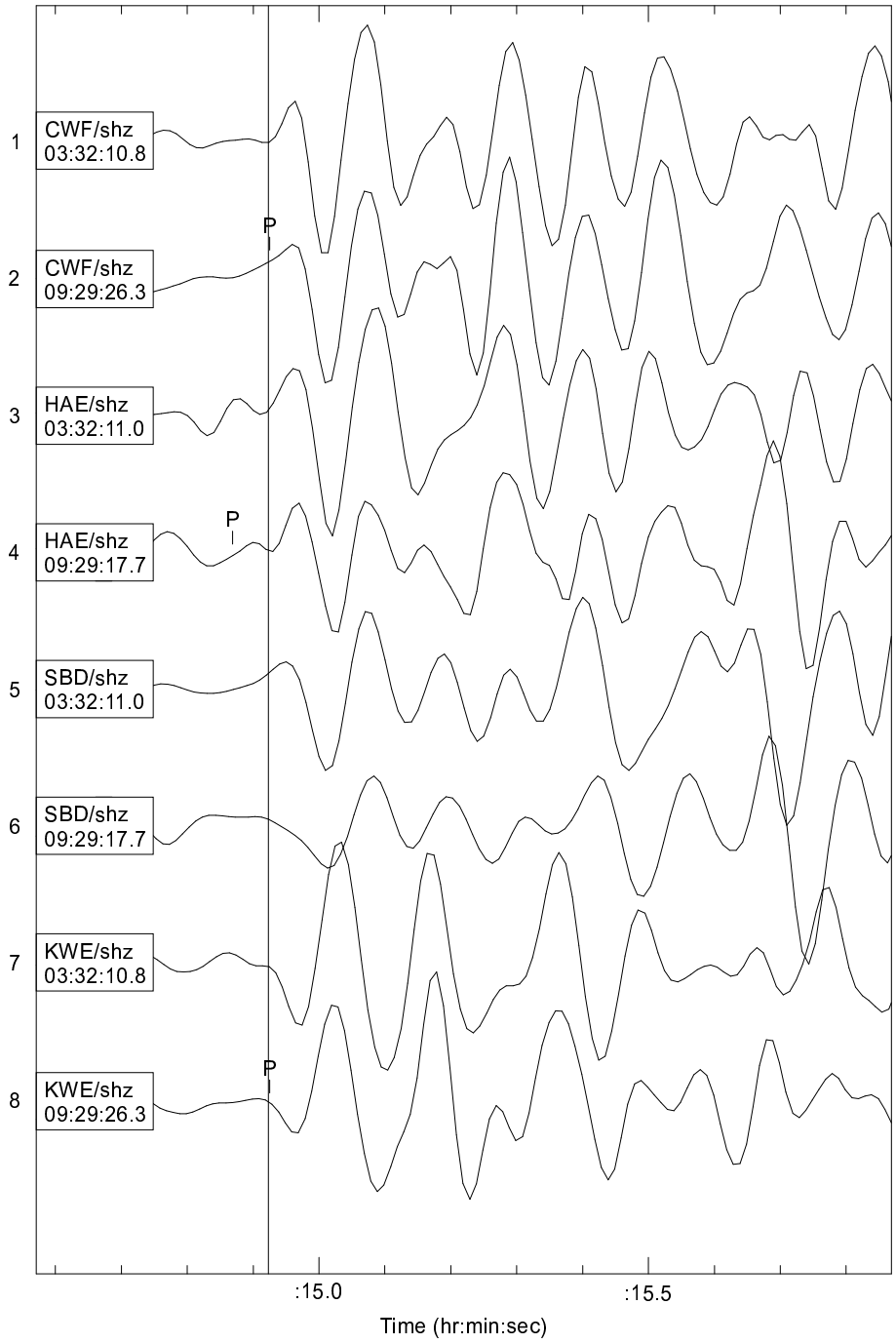

Figure 15: A comparison of the waveforms from the first aftershock at 03:32 UTC on 23 September and second aftershock at 09:29 UTC on 24 September at four stations CWF, HAE, SBD and KWE.

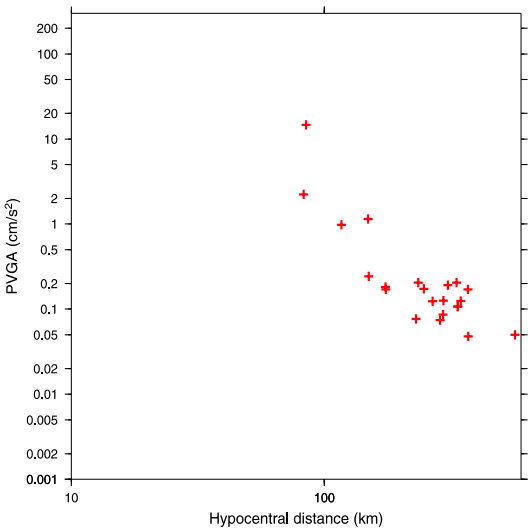

Figure 16: The decay of vertical ground acceleration (PVGA) with hypocentral distance for the mainshock.

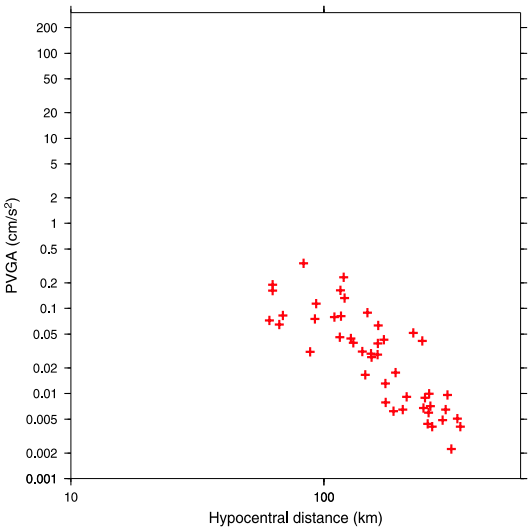

Figure 17: The decay of vertical ground acceleration (PVGA) with hypocentral distance for the largest aftershock.

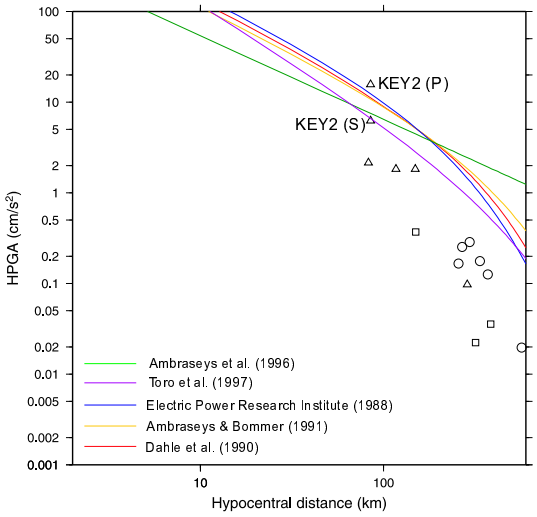

Figure 18: Observed values of peak horizontal ground acceleration (PHGA) from strong motion (triangles), short period (circles) and broadband instruments (squares), compared with the values predicted by various ground motion prediction relations.

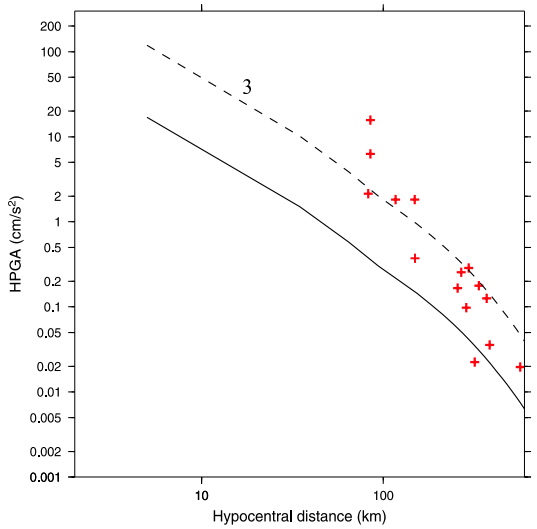

Figure 19: Comparison of observed PHGA for the mainshock with theoretical values using RVT. Crosses show the observed data. The solid black line shows PHGA calculated using average $\Delta\sigma$ and M_W from Table 3. The dashed line shows a more conservative estimate of PHGA calculated using the standard deviation on $\Delta\sigma$ and M_W.

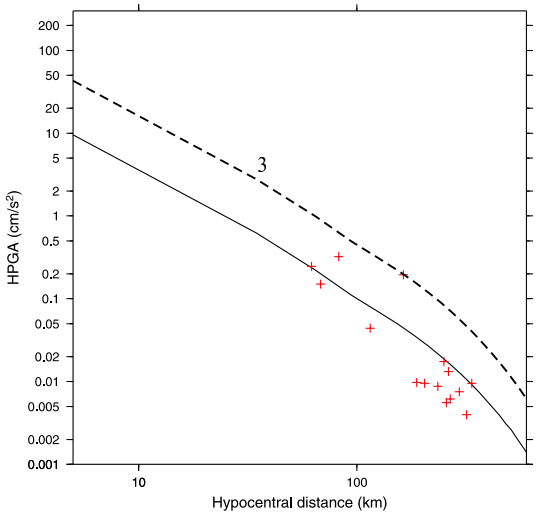

Figure 20: Comparison of observed and theoretical PHGA for the first aftershock. Crosses show the observed data. The solid black line shows PHGA calculated using average $\Delta\sigma$ and M_W from Table 4. The dashed line shows a more conservative estimate of PHGA calculated using the standard deviation on $\Delta\sigma$ and M_W.